




Generalized Langevin subdiffusion in channels: The bath always winsEugene B. Postnikov ^{*}*Department of Theoretical Physics, Kursk State University, Radishcheva St. 33, Kursk 305000, Russia
and Institute of Physics, Saratov State University, Astrakhanskaya St. 83, Saratov 410012, Russia*Igor M. Sokolov [†]*Institut für Physik and IRIS Adlershof, Humboldt-Universität zu Berlin, Newtonstraße 15, D-12489 Berlin, Germany* (Received 5 January 2024; revised 23 July 2024; accepted 12 August 2024; published 3 September 2024)

We consider subdiffusive motion, modeled by the generalized Langevin equation in an equilibrium setting, of tracer particles in channels of indefinite length in the x direction: the channels of varying width and the channels with sinusoidally meandering midline. The subdiffusion in the x direction is not affected by constraints put by the channel. This is especially astonishing for meandering channels whose centerline might be quite long. The same behavior is seen in a holonomic model of a bead on a sinusoidal and meandering wire, where some analytic insights are possible.

DOI: [10.1103/PhysRevE.110.034104](https://doi.org/10.1103/PhysRevE.110.034104)**I. INTRODUCTION**

The generalized Langevin equation (GLE) belongs to the basic approaches for modeling anomalous, in particular, subdiffusive transport processes in complex media [1,2]. The equation can in principle be derived from the underlying Hamiltonian dynamics of a complex system [3] (see, e.g., [4,5] for modern developments). It allows for a clear physical interpretation focused on the trajectories of individual particles' motion, and is a valuable tool in physics of polymers and living systems (e.g., at the subcellular scales) [6–9], giving their description at least on the phenomenological level (see [10,11] for reviews). The approach based on the GLE with a power-law memory kernel was applied for modeling subdiffusive intramolecular motion (see, e.g., [12,13]), and such equations should be kept in mind as a candidate for possible explanations of anomalous diffusion of tracers in biological fluids [14]. The GLEs with power-law memory kernels have many unusual and counterintuitive properties.

Considering the case of a GLE with a power-law memory kernel at equilibrium conditions (viscoelastic subdiffusion), Goychuk [15] revealed the independence of the asymptotic transport regime of the presence of periodic potential in one dimension. However, the one-dimensional structure does not allow for investigation of the role of boundary conditions and other constraints which may be crucial in many physical and biophysical situations. The only more or less investigated case corresponds to confined geometries (see, e.g., [16]).

In our previous work [17] we considered a homogenization problem for a subdiffusion, as described by the GLE in an equilibrium setting, in a two-dimensional array of solid obstacles. The main result of this work is that if

the infinite motion in the system is possible, the long-time (homogenized) behavior of the subdiffusion in such a system is the same as in a homogeneous medium without obstacles: not only the exponent but also the prefactor in the mean-squared displacement (MSD) stay the same as they were without obstacles. This finding is in stark contrast to what is observed in diffusion, where the diffusion coefficient is a monotonically decaying function of the packing fraction of the obstacles (see, e.g., [18]). In this work we discuss a simpler, quasi-one-dimensional situation for which the counterintuitive behavior of the subdiffusing tracers gets evident. The cases we have in mind correspond to diffusion in channels of indefinite length in the x direction and of different shapes: the channels of varying cross section and the meandering channels, motivated by a variety of biophysical situations.

The cases of channels of varying cross section include the transmembrane ion channels whose shape is modulated by surrounding proteins (see, e.g., [19]). Due to biological ubiquity, such situations for normal diffusion are considered in many works; Refs. [20,21] give a pick of recent examples. The transmembrane channels often exhibit anomalous diffusion but are typically short, which implies complex effects at entrance and exit, which we wanted to exclude by considering infinite ones.

A case of a long channel of varying width corresponds to pathological changes in the neuronal axons [22]. The axons give also examples for meandering channels, having undulated, approximately sinusoidal shape. Diffusion of intracellular metabolites inside axons is revealed by means of the diffusion-weighted magnetic resonance imaging (DW-MR) [23,24]. The conventional shape-dependent models operate with averaged apparent diffusion coefficients; there is, however, experimental evidence [25–27] that normal diffusion can only explain the short-time evolution of the DW-MR signal. For longer times, its multiexponential relaxation corresponds to an anomalous (subdiffusive) transport [28].

^{*}Contact author: postnikov@kursksu.ru[†]Contact author: igor.sokolov@physik.hu-berlin.de

Yet another example where the effects of boundaries can play a crucial role corresponds to the brain's extracellular space (ECS) filled by a physiological fluid comprising liquid solvent with a variety of macromolecular compounds. The transport through the ECS is heavily affected by its tortuosity but not completely understood even in the case of normal diffusion [29,30]. Recent experiments at the level of single-particle tracking and mesoscopic ensemble measurements hint onto subdiffusive motion [31,32].

In all these biological situations, there is a strong evidence for anomalous diffusion but, so far, no clear hints on a particular model of it. When discussing a particular model as a candidate for explanation of experimental findings, one should be aware of its properties [1,11]: The researcher should keep in mind that the ones of subdiffusion (as described by GLEs) in channels and meshes may be quite peculiar.

II. TRANSPORT IN FINITE-WIDTH CHANNELS

We start our discussion by considering the situation for a subdiffusion (as described by a GLE) in a two-dimensional channel of indefinite length in the x direction, bounded by the walls given by the two functions $y_u = f_u(x)$ and $y_l = f_l(x)$ where the subscripts u and l stand for “upper” and “lower,” i.e., a quasi-one-dimensional situation. We consider two paradigmatic cases: the “lakes and straits” situation of a symmetric channel of width periodically varying from its minimum value W to the maximal value $W + A$ (with A being the amplitude of modulation) with period L , and a case of a meandering channel with sinusoidal midline (typical width W , amplitude of meandering A , period L). The corresponding channels are shown in the upper panels of Figs. 1 and 2. For normal diffusion, the first situation is well investigated, and can be described by the Fick-Jacobs approach [33–36], and the second one is considered in [37,38]. For our case of subdiffusive motion, the second situation is of an utmost interest, stressing the difference in behavior of normal and anomalous diffusion. Special interest lies in the fact that the limiting case of a very narrow channel can be reduced to a one-dimensional situation of a bead diffusing on a sinusoidal wire, for which case the effective GLE in one dimension (1D) can be put down and investigated, which will be done in Sec. III.

The motion of the particle is described by the generalized Langevin equation in two dimensions in an equilibrium setting and with the isotropic noise,

$$M\ddot{\mathbf{x}}(t) + \int_0^t dt' \hat{K}(t-t')\dot{\mathbf{x}}(t') = \boldsymbol{\zeta}(t), \quad (1)$$

with M being the mass of the tracer particle, $\hat{K}(t)$ the memory kernel, and $\boldsymbol{\zeta}(t)$ being the noise term. The noise is assumed to be Gaussian, and to have zero mean. The coordinate $\mathbf{x} = (x, y)^T$ and the noise (random force) $\boldsymbol{\zeta}(t) = (\zeta_x(t), \zeta_y(t))^T$ are two-dimensional vectors, and the memory kernel $\hat{K}(t)$ is a matrix; in what follows we will consider the isotropic situation where ζ_x and ζ_y are two independent statistical copies of the Gaussian noise $\zeta(t)$, and the matrix $\hat{K}(t)$ is diagonal, with two equal entries $K(t)$. For equilibrium bath, the memory kernel and the correlation function of the noise $C_{\zeta,\zeta}(t) =$

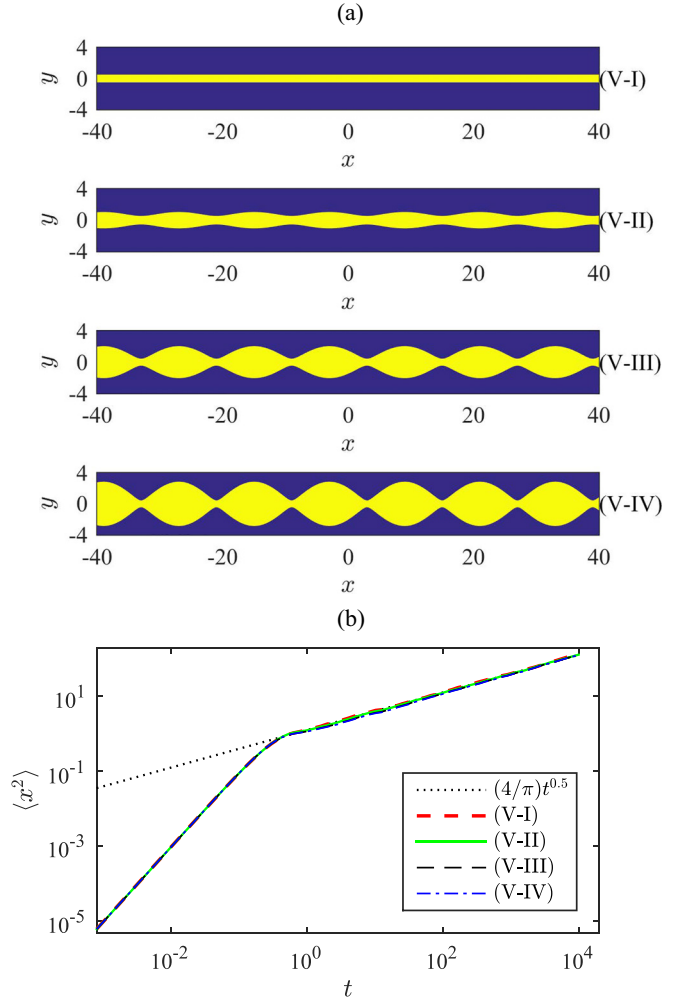


FIG. 1. The situation of the variable-width channel: (a) The straight channel, and three channels with the different width variations (the parameters are given in Appendix A). (b) The MSD for these four cases and the asymptotic subdiffusive dependence.

$\langle \zeta(t')\zeta(t'+t) \rangle$ fulfill the fluctuation-dissipation relation

$$k_B T K(t) = C_{\zeta,\zeta}(t) \quad (2)$$

for $t \geq 0$. For $t \geq 0$, the kernel $K(t)$ will be assumed to be a continuous function of t for all cases except for the purely diffusive one (with the white noise), when it tends to a δ function. Depending on the exact form of the kernel, the equation can describe a variety of diffusive, subdiffusive, and superdiffusive motions. Here, we concentrate on subdiffusion, although a diffusive case will be considered as well, for comparison. For subdiffusion, the free motion of the tracer at longer times corresponds to

$$\langle x^2(t) \rangle = \langle y^2(t) \rangle = D^* t^\alpha,$$

with $0 < \alpha < 1$, and with D^* being the prefactor connected with the (sub)diffusion coefficient. The kernel $K(t)$ follows a power law [17]

$$K(t) = \frac{1}{k_B T} C_{\zeta,\zeta}(t) = \frac{2k_B T}{D^*} \frac{\sin \pi \alpha}{\pi \alpha} t^{-\alpha} \equiv K_0 t^{-\alpha}.$$

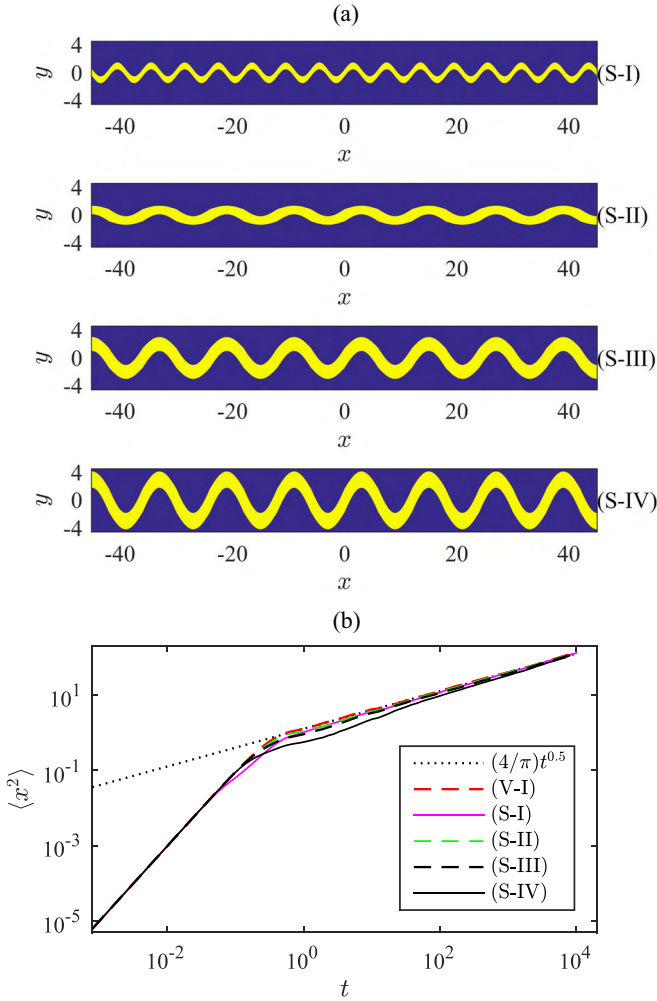


FIG. 2. Sinusoidally modulated channels: (a) The straight channel (V-I), the same as in Fig. 1(a), and three different shapes (the parameters are given in Appendix A). (b) The MSD for these cases and the asymptotic subdiffusive dependence. The parameters of the bath and initial conditions are the same as in Fig. 1.

In simulations for subdiffusion performed for the present work we use $\alpha = \frac{1}{2}$, $k_B T = 1$, and $K_0 = 1$ resulting in $D^* = 4/\pi$ in dimensionless units. The mass of the particle is set to $M = 0.1$. The method of simulations is detailed in Ref. [17], and is also shortly described in Appendix A.

Let us now pass to the *quasi*-1D situation. The walls of the channels are impenetrable for the diffusing tracer particle and correspond to a specular reflection of the tracer’s velocity on encounter with the wall, putting a nonholonomic constraint on the motion. The motion is readily modeled by a combination of Markovian embedding, as used in [15], and the “background field trick” for implementing the constraints [17]. The Markovian embedding method corresponds to modeling the bath by a collection of Ornstein-Uhlenbeck processes, and allows for a very economical implementation of the bath needing only some tens of overdamped harmonic oscillators driven by the white noise. We note that at difference to several situations involving polymers, the constraints on the tracer’s motion do not affect the bath.

Figure 1 presents the results of the simulations for the channel of varying width. The results for the straight channel allow to grasp the timescales: The transition from the ballistic regime to the subdiffusive one takes place at a time t_c slightly below unit time; further we note that the “mean free path” of the particle, i.e., the length $\lambda \sim \langle v^2 \rangle^{1/2} t_c$, is of the order or smaller than the minimal channel’s width, so that the motion in ballistic regime is hardly affected by the channel’s actual shape.

The simulation results show that the final (sub)diffusion along the x axis is not affected by the corrugation of the walls. This result could be guessed since the arrangement is very close to a one-dimensional version of the obstacle problem of Ref. [17] (large voids between the obstacles connected by narrow channels), and, moreover, infinite motion in the x direction is possible. One could argue the the motions in the y direction somehow decouple, and convince oneself that there is nothing astonishing and nothing to worry about. This argument, however, does not work for the case of a sinusoidal channel in the case of strong modulation, where the horizon of the free motion in the x direction is much smaller than the modulation period. These results are presented in Fig. 2.

One readily infers that while the shape of the channel plays the role at intermediate times, from the time when the motion leaves the ballistic and enters the subdiffusive regime to some upper crossover time corresponding to the (sub)diffusion time over a period of the channel ($\sim 10^2$ in our setup), at longer times the behavior is universal, and is not affected by the channel’s shape. Here there is already something to be astonished about: In spite of the strong modulation, the parameters of subdiffusion at longer time stay the same as they were for a straight channel.

Let us consider the the length of the midline of the channel between 0 and x , which is given by

$$s(x) = \int_0^x \sqrt{1 + m^2 \cos^2 \left(\frac{2\pi}{L} x' \right)} dx' = \frac{L\sqrt{1 + m^2}}{2\pi} E \left(\frac{2\pi x}{L} \middle| \frac{m^2}{m^2 + 1} \right) \quad (3)$$

with $E(u|z)$ being the elliptic integral of the second kind, Eq. 17.2.8 in Abramowitz and Stegun’s Handbook [39]), and with $m = 2\pi A/L$. Therefore, for large values of A the total length of the midline is considerably larger than the displacement in the x direction.

For $x \gg L$ the expression has a linear main asymptotics $s(x) = \kappa(m)x$. To see this, we first note that the integrand in Eq. (3) is strictly positive: The length of the midline is a monotonically growing function of x , and for large x we can approximate this length by interpolating between the values of x being the multiples of the period length, taking $x = Ln$. Since the integrand is essentially periodic with a shorter period $L/4$, we can then write

$$s(x = nL) = 4n \int_0^{L/4} \sqrt{1 + m^2 \cos^2 \left(\frac{2\pi}{L} x' \right)} dx',$$

and change the integration variable to $\xi = \frac{2\pi x'}{L}$:

$$\begin{aligned} s(x = Ln) &= Ln \frac{2}{\pi} \int_0^{\frac{\pi}{2}} \sqrt{1 + m^2 \cos^2 \xi} d\xi \\ &= Ln \frac{2}{\pi} \sqrt{1 + m^2} \int_0^{\frac{\pi}{2}} \sqrt{1 - \frac{m^2}{1 + m^2} \sin^2 \xi} d\xi \\ &= Ln \frac{2}{\pi} \sqrt{1 + m^2} E\left(\frac{m^2}{m^2 + 1}\right), \end{aligned}$$

where $E(x)$ is a complete elliptic integral of the second kind [39]. Therefore, the asymptotic proportionality coefficient between s and x [$s = \kappa(m)x$] is

$$\kappa(m) = \frac{2}{\pi} \sqrt{1 + m^2} E\left(\frac{m^2}{m^2 + 1}\right).$$

We note that for $m = 0$ one has $\kappa = 1$ and for $m \rightarrow \infty$ one has $\frac{2}{\pi} \sqrt{1 + m^2} E(1) \simeq \frac{2m}{\pi}$, so that for large amplitudes of modulation $s(x) \simeq (4A/L)x$.

If we consider an inclined straight channel at angle ϕ with the x axis, the subdiffusion in the x direction will be slower than the one along the midline since $\langle x^2(t) \rangle = \langle s^2(t) \rangle \cos^2 \phi$, i.e., the MSD $\langle x^2(t) \rangle$ at a given time will be by a factor $\cos^2 \phi$ smaller than in a horizontal channel. If we, however, bend the channel periodically in a manner of a folding rule, the MSD is the same as in a much shorter horizontal channel. This means that the (sub)diffusion along the midline of the modulated channel is essentially *considerably faster* than without modulation.

We note that the effect is only present for long-range memory kernels, and is absent in the case when the asymptotic behavior is diffusive: in this case the corresponding MSD in the x direction for a meandering channel is smaller than for a straight one. The simulation results for this case are presented in Fig. 6 in Appendix B, where also the corresponding discussion is given.

III. GENERALIZED LANGEVIN EQUATION FOR A BEAD ON A WIRE

To discuss the effect in its whole purity, we consider a situation with a holonomic constraint being a limiting case of a very narrow channel, i.e., a bead on a wire. We start from deriving the GLE for this case following the lines of the standard derivation of the GLE for a particle in a Kac-Zwanzig bath. The form of this equation is different from the standard one, Eq. (1), used in Sec. II. Then we proceed to show that our Markovian embedding procedure leads to exactly the same equation. In Sec. III C we present the results of simulation for the case of sinusoidal and meandering wires.

A. Hamiltonian system: Bath of harmonic oscillators

Let us consider a simple example, a system with holonomic constraint, a bead with mass M on a wire whose shape is given by a function $Y = Y(X)$, in a contact with the bath. The coordinates and momenta of the tagged particle (tracer) are denoted by capital letters (at difference to the previous text), the ones of the bath particles by the small ones. Parametrization by the length of the wire s leads to the simplest form of the

kinetic energy of the bead which is coordinate independent. In this case, an effective one-dimensional GLE can be derived. One considers the bath of harmonic oscillators (Kac-Zwanzig bath [3]), i.e., the Hamiltonian situation, and eliminates the bath variables [3,40,41].

In more detail, we start from a simple Hamiltonian model which is used for establishing the standard GLE (the Kac-Zwanzig model, where the bath is considered as an ensemble of harmonic oscillators thermalized at the beginning [3]), and repeat the steps now using generalized coordinate for the test particle.

The origin $s = 0$ coincides with $X = 0$, and the position of the tracer is parametrized as $\mathbf{R} = (X(s), Y(s))^T$. The bath is considered as a Galilean-invariant (Kupferman's) bath [40] of harmonic oscillators coupled bilinearly both to X and to Y coordinates. The total Hamiltonian of the system reads as

$$\begin{aligned} H &= \frac{P^2}{2M} + \sum_i \left\{ \frac{p_i^2}{2m_i} + \frac{1}{2} m_i \omega_i^2 [(X(s) - x_i)^2 \right. \\ &\quad \left. + [Y(s) - y_i]^2] \right\}, \end{aligned}$$

with P being the generalized momentum conjugated to s . The Hamiltonian equations of motion for our system read as

$$\begin{aligned} \dot{P} &= -\frac{\partial H}{\partial s} = \frac{dX}{ds} \left[-\left(\sum_{j=1}^N k_j \right) X(s) + \sum_j k_j x_j \right] \\ &\quad + \frac{dY}{ds} \left[-\left(\sum_{j=1}^N k_j \right) Y(s) + \sum_j k_j y_j \right] \end{aligned} \quad (4)$$

with $k_j = m_j \omega_j^2$ and

$$\dot{p}_{j,x} = -\frac{\partial H}{\partial x_j} = -k_j x_j + k_j X(s), \quad (5)$$

$$\dot{p}_{j,y} = -\frac{\partial H}{\partial y_j} = -k_j y_j + k_j Y(s). \quad (6)$$

Taking into account that $P = M\dot{s}$ and that $p_j = m_j \dot{q}_j$ and dividing the both parts of Eqs. (5) and (6) by m_j we obtain the final equations of motion

$$\begin{aligned} M\dot{s} &= \frac{dX}{ds} \left[-\left(\sum_{j=1}^N k_j \right) X(s) + \sum_j k_j x_j \right] \\ &\quad + \frac{dY}{ds} \left[-\left(\sum_{j=1}^N k_j \right) Y(s) + \sum_j k_j y_j \right] \end{aligned} \quad (7)$$

and

$$\ddot{q}_j = -\omega_j^2 q_j + \omega_j^2 Q(s), \quad (8)$$

where, in the second equation, q_j is either x_j or y_j and Q is X or Y , respectively, and denote $Q[s(t)]$ by $Q(t)$ for simplicity.

We note that the bath equations do not depend on the choice of the generalized coordinates for the bead. We start from Eq. (8). The general solution to this equation for given

$Q(t)$ is

$$q_j(t) = q_j(0) \cos \omega_j t + \dot{q}_j(0) \frac{\sin \omega_j t}{\omega_j} + \omega_j \int_0^t dt' Q(t') \sin \omega_j(t-t').$$

Performing integration by parts,

$$\int_0^t dt' Q(t') \sin \omega_j(t-t') = Q(t') \frac{\cos \omega_j(t-t')}{\omega_j} \Big|_0^t - \int_0^t dt' \dot{Q}(t') \frac{\cos \omega_j(t-t')}{\omega_j},$$

we restore the explicit dependence on the initial position $Q(0)$:

$$q_j(t) = [q_j(0) - Q(0)] \cos \omega_j t + \dot{q}_j(0) \frac{\sin \omega_j t}{\omega_j} + Q(t) - \int_0^t dt' \dot{Q}(t') \cos \omega_j(t-t')$$

with $\dot{Q}(t) = \frac{dQ}{dt} = \frac{dQ}{ds} \dot{s}$. We now introduce this solution into Eq. (7):

$$\begin{aligned} M\ddot{s} &= \frac{dX}{ds} \left[- \left(\sum_{j=1}^N k_j \right) X(t) + \sum_j k_j X(t) \right] \\ &\quad - \frac{dX}{ds} \sum_j k_j \int_0^t dt' \dot{X}(t') \cos \omega_j(t-t') \\ &\quad + \frac{dX}{ds} \sum_j k_j \left\{ [x_j(0) - X(0)] \cos \omega_j t + \dot{x}_j(0) \frac{\sin \omega_j t}{\omega_j} \right\} \\ &\quad + \text{similar terms containing } y \text{ and } Y. \end{aligned}$$

The two terms in the first line cancel. This equation has the structure of a Newton's equation with the friction term keeping the memory on the previous particle's velocities:

$$\begin{aligned} M\ddot{s} &= - \frac{dX}{ds} \int_0^t dt' \dot{X}(t') K(t-t') \\ &\quad - \frac{dY}{ds} \int_0^t dt' \dot{Y}(t') K(t-t') \\ &\quad + \frac{dX}{ds} F_1(t) + \frac{dY}{ds} F_2(t) \end{aligned} \quad (9)$$

with $\dot{X}(t') = \frac{dX}{ds} \dot{s}$ calculated for the position s at time t' and the same for Y . We can interpret it as a generalized (non-Markovian) Langevin equation, if we say that the forces $F_1(t), F_2(t)$ are fluctuating so strongly that they can be assumed random. Here $K(t)$ is the friction memory kernel

$$K(t) = \sum_j m_j \omega_j^2 \cos \omega_j t$$

(note that $K(t)$ has a dimension of the elastic constant, namely, $[K(t)] = \text{MT}^{-2}$) and $F(t)$ is the "noise" force

$$F(t) = \sum_j m_j \omega_j^2 \left[[q_j(0) - X(0)] \cos \omega_j t + \dot{q}_j(0) \frac{\sin \omega_j t}{\omega_j} \right].$$

Now we fix $X(0)$ and $Y(0)$ and equilibrate the bath at temperature T by connecting it to an additional external bath which is then removed (a harmonic bath, being integrable, does not equilibrate by itself).

We note that other kinds of initial equilibration procedures can be assumed, leading to an initial "glitch" or "slip" [41] as we will observe in our next variant of the model. In such an equilibrated bath we get

$$\langle q_j(0) - Q(0) \rangle = 0, \quad \langle p_j(0) \rangle = 0$$

(with p_j being either $p_{j,x}$ or $p_{j,y}$) and, according to the equipartition theorem,

$$m\omega_j^2 \langle [q_j(0) - Q(0)]^2 \rangle = k_B T, \quad \langle p_j^2(0) \rangle = k_B T m,$$

while all second cross moments $\langle \tilde{q}_i p_j \rangle$ [with $\tilde{q}_j = q_j(0) - Q(0)$] for all i, j , and $\langle \tilde{q}_i \tilde{q}_j \rangle, \langle p_i p_j \rangle$ with $j \neq i$ vanish. Now we evaluate the autocorrelation function of $F(t)$, say,

$$\begin{aligned} \langle F_1(t) F_1(t') \rangle &= \langle F_2(t) F_2(t') \rangle \\ &= \sum_j m_j^2 \omega_j^4 \left[\langle \tilde{q}_j^2(0) \rangle \cos \omega_j t \cos \omega_j t' \right. \\ &\quad \left. + \langle p_j^2(0) \rangle \frac{\sin \omega_j t \sin \omega_j t'}{m_j^2 \omega_j^2} \right] \\ &= \sum_j m_j^2 \omega_j^4 \left[\frac{k_B T}{m_j \omega_j^2} \cos \omega_j t \cos \omega_j t' \right. \\ &\quad \left. + \frac{k_B T}{m_j \omega_j^2} \sin \omega_j t \sin \omega_j t' \right] \\ &= \sum_j m_j \omega_j^2 k_B T \cos \omega_j(t-t') = k_B T K(t-t') \end{aligned} \quad (10)$$

and $\langle F_1(t) F_2(t') \rangle = 0$. This is a corresponding fluctuation-dissipation relation (of the second kind) for our non-Markovian Langevin equation (9), which is, however, highly nonlinear.

B. GLE for a bead on the wire from Markovian embedding

Let us now check whether our Markovian embedding solves exactly the equation we have devised in the previous section. In Markovian embedding we approximate the kernel with the sum of exponentials

$$K \simeq \sum_{n=0}^N \eta_n \exp(-\nu_n t). \quad (11)$$

Now, a system of overdamped oscillators (i.e., of Ornstein-Uhlenbeck processes), each in its own bath, is coupled to the bead which can only move in the direction of the wire. The forces exerted by the bath oscillators on a bead are given by

$$f_\gamma = \sum_{n=0}^N u_{n,\gamma}$$

(with u being the oscillators' coordinates and γ numbers the Cartesian components), like in Appendix A. The motion

normal to the wire is prevented by normal forces of reaction, and therefore the bath force with components f_x and f_y enters the equation of motion of a bead as

$$M\ddot{s} = \left(\frac{dX}{ds}\right)f_x + \left(\frac{dY}{ds}\right)f_y, \quad (12)$$

while the equations of motion of the oscillators read as

$$\dot{u}_{n,\gamma} = -\eta_n v_\gamma - v_n u_{n,\gamma} + \sqrt{2v_n \eta_n k_B T} \xi_{n,\gamma},$$

where the projections of the bead's velocity are

$$v_x = \left(\frac{dX}{ds}\right)\dot{s} \quad \text{and} \quad v_y = \left(\frac{dY}{ds}\right)\dot{s}.$$

Now we can formally integrate the equations of motion of the bath particles assuming $v_\gamma(t)$ known:

$$u = u(0)e^{-\nu t} + \int_0^t [\sqrt{2v_n \eta_n k_B T} \xi(t') - \eta v(t)] e^{-\nu(t-t')} dt'$$

(the indices n and γ are omitted), take

$$f_x = \sum_{n=0}^N u_{n,1}, \quad f_y = \sum_{n=0}^N u_{n,2}$$

and substitute the formal solutions for $u_{n,\gamma}$:

$$\begin{aligned} M\ddot{s} = & \sum_n \left\{ \left(\frac{dX}{ds}\right) u_n(0) e^{-\nu n t} \right. \\ & - \left(\frac{dX}{ds}\right) \int_0^t \left[\eta_n \left(\frac{dX}{ds}\right) \dot{s} \right] e^{-\nu_n(t-t')} dt' \\ & + \left(\frac{dX}{ds}\right) \int_0^t [\sqrt{2v_n \eta_n k_B T} \xi(t')] e^{-\nu_n(t-t')} dt' \left. \right\} \\ & + \text{similar terms for } Y. \end{aligned}$$

Using Eq. (11), we recognize in the second term the memory friction. The first term is a ‘‘slip’’ [41], which is zero on the average, but nonzero in each particular realization. The ‘‘slip’’ should be included into the noise term, and the sum of the first and the third terms gives us the stationary noise with the correlation function fulfilling the FDR provided $\langle u_n^2(0) \rangle = \eta_n k_B T$.

C. Simulation results for sinusoidal and meandering channels

In our simulations, the wire's shape is defined parametrically by the following system of equations:

$$X = s - B \sin\left(\frac{2\pi s}{L}\right), \quad (13)$$

$$Y = A \sin\left(\frac{2\pi s}{L}\right). \quad (14)$$

In this case, the parameters A and L determine the amplitude and period of the wire's oscillations; the parameter B determines an emergence of loops: for $B = 0$ the wire has sinusoidal shape $Y = A \sin\frac{2\pi X}{L}$. For $B = (L/2\pi)/2$ a periodic set of points where the wire is vertical, $dY/dX = \infty$, emerges, and for $B > (L/2\pi)/2$ the wire has meandering shape (the projections of the wire onto the x axis are nonunique). The

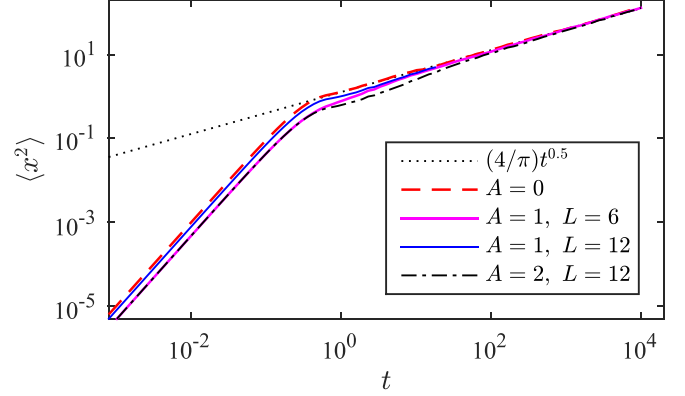


FIG. 3. The MSD of a bead on a sinusoidal wire whose shape is given by $Y(X) = A \sin(2\pi X/L)$. The parameters of the bath are the same as used in Figs. 1 and 2.

derivatives $\frac{dX}{ds}$ and $\frac{dY}{ds}$ for the coordinates given by Eqs. (13) and (14) are

$$\begin{aligned} \frac{dX}{ds} &= 1 - 2B \frac{2\pi}{L} \cos\left(\frac{2\pi}{L}s\right), \\ \frac{dY}{ds} &= A \frac{2\pi}{L} \cos\left(\frac{2\pi}{L}s\right). \end{aligned}$$

We start from thermalized u and $V = \dot{s}$ (and $s = 0$) and integrate

$$\begin{aligned} \dot{u}_{n,X} = & -\eta_n \left[1 - 2B \frac{2\pi}{L} \cos\left(\frac{2\pi}{L}s\right) \right] V - v_n u_{n,X} \\ & + \sqrt{2v_n \eta_n k_B T} \xi_{n,X}, \end{aligned} \quad (15)$$

$$\begin{aligned} \dot{u}_{n,Y} = & -\eta_n A \frac{2\pi}{L} \cos\left(\frac{2\pi}{L}s\right) V - v_n u_{n,Y} \\ & + \sqrt{2v_n \eta_n k_B T} \xi_{n,Y}, \end{aligned} \quad (16)$$

where the notation $\dot{s} = V$ is introduced, and then

$$\begin{aligned} M\dot{V} = & \left[1 - 2B \frac{2\pi}{L} \cos\left(\frac{2\pi}{L}s\right) \right] \sum_{n=0}^N u_{n,X} \\ & + A \frac{2\pi}{L} \cos\left(\frac{2\pi}{L}s\right) \sum_{n=0}^N u_{n,Y}. \end{aligned} \quad (17)$$

Integrating the obtained V and substituting s in Eq. (13), we get the desired distribution of walker's projections allowing the determination of the MSD dependence on time.

1. Sinusoidal wire

Let us start from the case of a wire having sinusoidal shape $y = A \sin\frac{2\pi x}{L}$. The results of simulations for a bead on the wire in a contact with exactly the same bath as before, in Sec. II, are shown in Fig. 3. For long times, this figure reproduces practically the same behavior as the one in the narrow channel, Fig. 2. The shift of the curves (on double-logarithmic scales) in the ballistic regime is due to the fact that now the ballistic motion corresponds not to the free one, but to the one on the inclined wire (so the corresponding velocity is not $\langle v^2 \rangle^{1/2}$ but $\langle v_x^2 \rangle^{1/2}$).

The corresponding result for an exponentially decaying kernel is presented in Fig. 7 of Appendix B: in this case the terminal diffusion coefficient is diminished exactly by a factor $\kappa^2(m)$, as it should be. We note that in our parametrization for this case $(dX/ds)^2 + (dY/ds)^2 = 1$, and see that for the case of a white noise with $K(t) = \gamma\delta(t)$ the equation reduces to a simple one for an underdamped particle in a generalized coordinate s , $M\ddot{s} = -\gamma\dot{s} + \sqrt{2\gamma k_B T}\xi$. This is the terminal situation for other integrable kernels leading to a Markovian limit.

For subdiffusion, the kernel is not integrable, and the integrals are dominated by the long-time behavior of K . If a motion of a bead on the inclined straight wire is considered, $dX/ds = \cos\phi$ and $dY/ds = \sin\phi$ are constant, and the equation reduces to the one-dimensional GLE for the motion along the wire, $M\ddot{s}(t) + \int_0^t dt' \hat{K}(t-t')\dot{s}(t') = \zeta(t)$, with $\zeta(t)$ being a single noise fulfilling Eq. (2). The projection on the x axis then corresponds to a slower (sub)diffusion than along the wire.

The situation with a sinusoidal wire is different. Assuming that the dynamics at long times is described by the overdamped limit of Eq. (9), i.e., that its left-hand side can be set to zero, we can divide both parts of the equation by $dX/ds > 0$, which is equivalent to introducing x as a generalized coordinate. We get

$$\begin{aligned} \int_0^t dt' \dot{X}(t')K(t-t') + \frac{dY}{dX}\bigg|_t \int_0^t dt' \left(\frac{dY}{dX}\bigg|_{t'} \right) \dot{X}(t')K(t-t') \\ = \zeta_x(t) + \frac{dY}{dX}\bigg|_t \zeta_y(t). \end{aligned} \quad (18)$$

In the second integral, the slowly decaying memory kernel is weighted with the trajectory-dependent oscillating function $\frac{dY}{dX}\big|_t \frac{dY}{dX}\big|_{t'}$, and the same weight appears in the correlation function of the second noise. Then, a plausible explanation of our numerical findings is that these oscillations effectively lead to vanishing of the corresponding contributions under integration for long-time lags, leaving us with the equation for unperturbed motion in the x direction. However, the mathematical proof of this vanishing is missing: We would be happy if the problem attracts attention of mathematically oriented researchers.

2. Meandering wire

The case of $B > L/4\pi$, with two examples of which are depicted in Fig. 4 (M-II) and (M-III), is more sophisticated. We note that in this case X can hardly be used as a generalized coordinate due to its nonuniqueness, and the discussion around Eq. (18) gets inapplicable.

Simulations were carried out by direct numerical integration of Eqs. (15)–(17) with the time step $dt = 10^{-3}$ and the statistical ensemble of 10^4 realizations. In this set of simulations, the initial thermalized velocities were aligned with the tangent to a wire at the starting point of motion (at the origin of coordinates).

Results of simulations corresponding to the shapes depicted in Fig. 4 in comparison with the same on a straight line are presented in Fig. 5. One can see that asymptotic universality of the MSD's time dependence persists in this case too, while the short-time behavior is different. For the

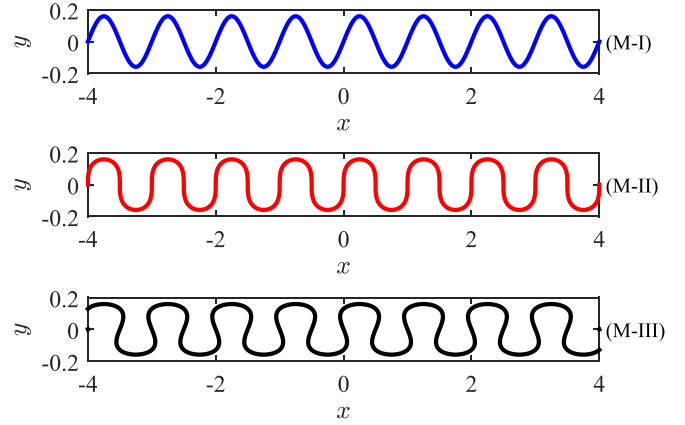


FIG. 4. Examples of meandering channels corresponding to Eqs. (13) and (14) with $L = 1$ and $A = 1/(2\pi)$, $B = 0$ (M-I), $A = 1/(2\pi)$, $B = 0.5/(2\pi)$ (M-II), and $A = B = 1/(2\pi)$ (M-III).

case shown in Fig. 4 (M-II) the particle starts at a practically vertical portion of the curve, and does not show any ballistic motion at all in projection on the x axis (at short times the particle moves only in vertical direction). The projection of its position onto the x axis shows a “superaccelerated” motion corresponding to leaving the vertical part of the curve and acquiring a nonzero x coordinate. In the case of a significantly meandering channel, Fig. 4 (M-III), the ballistic motion at short time is present, and the oscillation of the MSD around the behavior corresponding to the straight wire corresponds to the change in the direction of motion along the x axis when the coordinate s continuously grows. For longer times, these effects die out due to averaging, leading to the universal behavior which sets on after the particle has diffused over a period of the curve.

IV. CONCLUSIONS

We simulated subdiffusive motion of particles, as described by generalized Langevin equation with equilibrium bath, in quasi-one-dimensional channels of two geometries: the channels of varying width, and meandering ones. In both cases, the final regime of the transport along the x direction is not

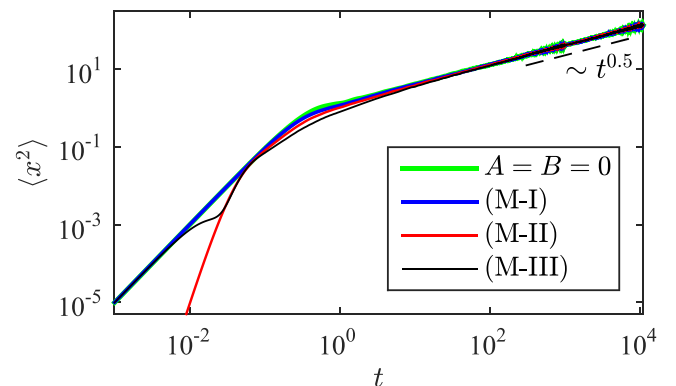


FIG. 5. The MSD of a bead on meandering wires whose shape is in Fig. 4. The parameters of the bath are the same as used in Figs. 1–3.

affected by modulation, i.e., is governed only by the properties of the bath: “The bath always wins.” This is especially astonishing for sinusoidal channels with finite horizon since the length of the midline of the channel corresponding to the displacement Δx is considerably longer than Δx . The effect is associated with slowly decaying kernels, and is absent in the diffusive motion. Going to the limit of narrow channels, one could consider a holonomic situation (a bead on either a sinusoidal or a meandering wire) for which the effective GLE can be put down and simulated, showing a very similar behavior. The situation might be of importance for subdiffusive motions of particles in constrained (but not confined) geometries, if the constraint on the particle does not affect the bath: Discussing experimental results on subdiffusive motion in complex geometries one should keep in mind the existence of situations when the geometry of constraints ceases to matter. These situations should be distinguished from cases of polymers’ motion in a channel or their reptation, where the molecule (being a part of the bath for a tagged particle whose position is monitored) is affected by constraints.

ACKNOWLEDGMENT

E.B.P. was supported by the Russian Science Foundation, Project No. 22-15-00143.

APPENDIX A: SIMULATION ALGORITHM FOR FINITE-WIDTH CHANNELS

To simulate subdiffusion in two-dimensional channels with impenetrable walls, the two-step algorithm with fictional “background field” proposed in the work [17] was used. It modifies the Euler-Maruyama explicit scheme applied to the system representing the GLE via the bath of N two-dimensional Ornstein-Uhlenbeck processes

$$\begin{aligned} \dot{x}_\gamma &= v_\gamma, \\ M\dot{v}_\gamma &= \sum_{n=0}^N u_{n,\gamma}, \end{aligned} \quad (\text{A1})$$

$$\dot{u}_{n,\gamma} = -\eta_n v_\gamma - \nu_n u_{n,\gamma} + \sqrt{2\nu_n \eta_n k_B T} \xi_{n,\gamma},$$

where γ numbers the Cartesian components, η_n and ν_n are parameters of the Markovian embedding (see [17] and below), M is the particle’s mass, and T is the system’s temperature (in simulations we use $M = 0.1$ and $k_B T = 1$).

The choice of ν_n is $\nu_n = \nu_0 b^{-n}$, and $\eta_n = C(\alpha, b) \nu_n^\alpha$, with $\nu_0 = 10^3$ and $C \approx 1.2874$, was like in [17]. We use the decade scaling $b = 10$ with $N = 16$ components per coordinate. Our simulation parameters are $\alpha = 0.5$ (relatively deep in the subdiffusion domain), $M = 0.1$, $k_B T = 1$, and $K_0 = 1$. The initial conditions correspond to centered Gaussian distributions of v and $u_{n,\alpha}$ with $\langle v_\alpha(0)^2 \rangle^{1/2} \equiv \sqrt{k_B T / M} = \sqrt{10}$, and $\langle u_{n,\alpha}(0)^2 \rangle^{1/2} = \sqrt{\eta_n K_B T}$. The tracer starts at the origin of the coordinate system.

The modification of Euler-Maruyama integrator is as follows: Each step of integration Δt (it was taken 10^{-4} for $t < 1$ and 10^{-3} otherwise) corresponds to adding the corresponding random Gaussian variables to the bath variables $u_{n,\alpha}$, and updating $u_{n,\alpha}$, and the tracer’s velocity and position. This

initial scheme would approximate the trajectory of the tracer by segments of straight lines between $\mathbf{x}(t) = (x(t), y(t))$ and $\mathbf{x}(t + \Delta t) = (x(t + \Delta t), y(t + \Delta t))$.

To account for specular reflections, each time step Δt is subdivided into smaller substeps $dt = \Delta t / 10$, which correspond to subdivision of each such segment into 10 subsegments of the same length numbered by $n = 1, \dots, 10$, since the tracer’s velocity on a segment is not updated.

The boundaries of the channel are defined by level lines of a function $G(x, y)$, which we call the “background field.” For each point of this subdivision $\mathbf{x}(t + ndt)$, we calculate the value of the indicator function $g(\mathbf{x})$,

$$g(x, y) = -\frac{1}{2} \{ \text{sign}[G(x, y) - l] + 1 \}, \quad (\text{A2})$$

which is equal to 0 within the channel and -1 outside of it. Here l is the “height” of the level. The normal to the channel’s boundary is given by the normalized gradient $\mathbf{A}(\mathbf{x}_h) = -\nabla G(\mathbf{x}_h) / |\nabla G(\mathbf{x}_h)|$ of the field G at the hitting point \mathbf{x}_h . Starting from the beginning of the i th step at t_i we calculate approximate positions $\mathbf{x}_n = \mathbf{x}(t_i) + \mathbf{v}(t_i)ndt$, $n = 1, \dots, 10$, and the corresponding values of $g_n = g(\mathbf{x}_n)$. The time from the beginning of the step to hitting the boundary is then $\Delta t' = \Delta t + dt \sum_{n=1}^{10} g_n$ and the position at which the particle hits the obstacle is

$$\mathbf{x}_h = \mathbf{x}(t_i) + \mathbf{v}(t_i) \left(\Delta t + dt \sum_{n=1}^{10} g_n \right).$$

Now we can update the position

$$\mathbf{x}(t_{i+1}) = \mathbf{x}_h + \mathbf{V} \left(\Delta t + dt \sum_{n=1}^{10} g_n \right),$$

where \mathbf{V} is the velocity after reflection given by

$$\mathbf{V} = \mathbf{v}(t_i) + 2\mathbf{A}|\mathbf{A} \cdot \mathbf{v}(t_i)|.$$

Now one can update the particle’s velocity

$$\mathbf{v}(t_{j+1}) = \mathbf{V} + \sum_k \mathbf{u}_n(t_j) \Delta t,$$

and, finally, the bath variables

$$\mathbf{u}_n(t_{j+1}) = \mathbf{u}_n(t_j) - [\eta_n \mathbf{v}(t_{j+1}) + \nu_k \mathbf{u}(t_j)] \Delta t + \sigma \Xi \sqrt{\Delta t},$$

with Ξ being a Gaussian variable with zero mean and unit variance, and $\sigma = \sqrt{2\nu_n \eta_n k_B T}$.

For different channel shapes we use the following background field functions:

$$G(x, y) = d \sin \left(\frac{2\pi x}{L} \right) + y^2$$

for the case of the variable-width channel,

$$G(x, y) = \left[y - d \sin \left(\frac{2\pi x}{L} \right) \right]^2$$

for (S-I) and

$$G(x, y) = \left[y - d \sin \left(\frac{2\pi x}{L} \right) \right]^2 + \frac{d}{2} \left| \sin \left(\frac{2\pi x}{L} \right) \right|$$

for (S-II) to (S-IV), respectively. Here, the second term is added to partly compensate the difference in the thickness

TABLE I. List of parameters defining the channel's shape.

Channel	d	L	l
(V-I)	0		1
(V-II)	0.4	12	0.7
(V-III)	2	12	2.2
(V-IV)	4	12	4.2
(S-I)	1	6	0.25
(S-II)	0.75	12	0.75
(S-III)	2	12	2
(S-IV)	3	12	2.9

of the channel in the direction normal to its midline at different x .

The parameters d and L , and the parameter l in Eq. (A2) are given in Table I.

APPENDIX B: DIFFUSIVE CASE

The diffusion situation is mimicked by switching off all bath oscillators except for the fastest one, now producing the noise with exponentially decaying (i.e., integrable) correlation function of the noise and the memory kernel $K(t) = \eta \exp(-\nu t)$ with $\nu = \nu_0$ and $\eta = C(\alpha, b)\nu_0^g$.

The results for the same channels as in Fig. 2 of the main text are shown in Fig. 6 below, and the terminal behavior corresponds indeed to a slower diffusion than in the straight channel, i.e., to $D < D(0)$ with $D(0)$ being the diffusion coefficient in the straight channel.

The value of $D(0)$ can be obtained from the general expression for the MSD [Eq. (8) of Ref. [17]], with the function $H(t)$ given by its Laplace transform $H(s)$ [Eq. (4) of the same work]. Since only the long-time asymptotic of the MSD is needed, the function $H(s)$ can be approximated in the leading order in s for $s \rightarrow 0$. The result is $D(0) = k_B T \nu / \eta$, and in

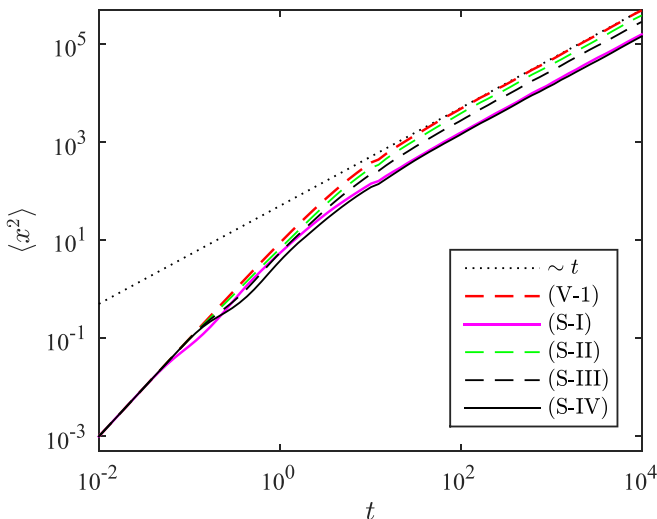


FIG. 6. The MSD in sinusoidally modulated channels in the diffusive regime, as obtained by switching off all bath oscillators except for the “fastest” one. Note the double-logarithmic scales.

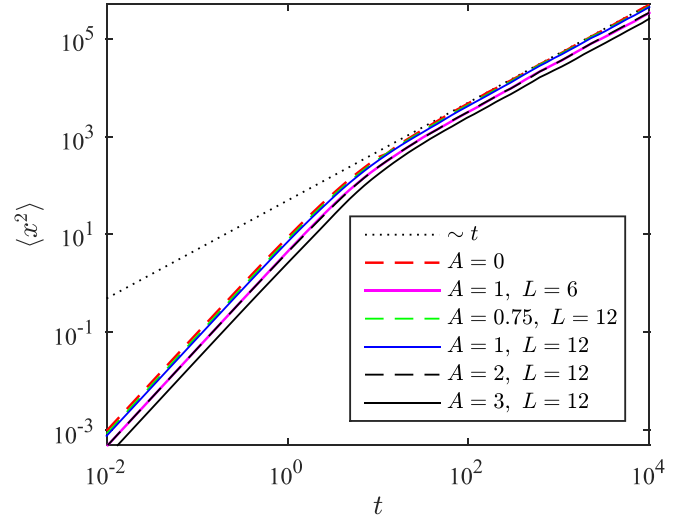


FIG. 7. The MSD on a sinusoidally modulated wire in the diffusive regime, as obtained by switching off all bath oscillators except for the “fastest” one.

our case is equal to $D(0) \approx 25$. The corresponding behavior is indicated in the figure by a thin dotted line.

The slowdown of diffusion in meandering channels is due to two factors: to the meandering of the centerline, and to the variation of the channel's width. The effect of width variation (leading to diffusion in presence of entropic barriers) is well investigated (see, e.g., [42]), while the combination of width modulation with curved midline was considered only relatively recently [37]. Both effects lead to slowdown of diffusion, but the expressions for the terminal diffusion coefficient are simple only for narrow channels, which is not the case in our simulations.

The effect of meandering midline can be, however, considered in all its purity for a one-dimensional situation of a bead on a wire, in which case $D = \kappa^{-2}(m)D(0)$ [with the parameter $\kappa(m)$ defined in the main text]. For normal diffusion, this case indeed corresponds to a limit of narrow meandering channel of a constant width, a so-called serpentine channel [37,38].

The simulations for the case of a bead on a wire corresponding to the same parameters as in Fig. 3 of the main text are presented in Fig. 7. This case corresponds to the contribution of the length of the midline only. The wires considered correspond to centerlines of channels S-I to S-IV, and to an additional wire with $A = 1, L = 12$ showing a slightly stronger modulation than the centerline than S-II.

To stress the change of the terminal diffusion coefficient due to modulation we compared the numerical results with the ones obtained in calculations. The results of such comparison are given in Table II. The table shows the corresponding values of $\kappa^2(m)$ and the values of the reduced asymptotic diffusion coefficient, i.e., of the ratio

$$\tilde{D} = \frac{D_{A,L}}{D_0} \kappa^2(m) \quad (\text{B1})$$

with the values $D_{A,L}$ obtained by a linear fit $\langle x^2 \rangle = 2D_{A,L}t$ of the data presented in Fig. 7 for $10^3 < t < 10^4$. The table shows that the corresponding ratio is unity within the statistical uncertainty.

TABLE II. The reduced asymptotic diffusion coefficient, Eq. (B1), for the bead-on-the wire model.

A	L	$\kappa^2(m)$	\tilde{D}
1	6	1.523	1.002
0.75	12	1.076	0.982
1	12	1.135	1.045
2	12	1.523	1.022
3	12	2.142	1.091

For comparison, we show in Table III the values of \tilde{D} for thick sinusoidal channels corresponding to the results shown

TABLE III. The reduced asymptotic diffusion coefficient for “thick” channels with sinusoidal centerline.

Channel	\tilde{D}
(S-I)	0.48
(S-II)	0.85
(S-III)	1.2
(S-IV)	0.63

in Fig. 6. These may differ from unity considerably, showing that the meandering of the centerline might or might not be the main source of change in diffusion coefficient.

- [1] Y. Meroz and I. M. Sokolov, *Phys. Rep.* **573**, 1 (2015).
- [2] M. A. F. dos Santos, *Chaos, Solitons Fractals* **124**, 86 (2019).
- [3] R. Zwanzig, *Nonequilibrium Statistical Mechanics* (Oxford University Press, Oxford, 2001).
- [4] C. Ayaz, L. Scalfi, B. A. Dalton, and R. R. Netz, *Phys. Rev. E* **105**, 054138 (2022).
- [5] R. R. Netz, *Phys. Rev. E*, **110**, 014123 (2024).
- [6] I. Goychuk, in *Advances in Chemical Physics*, edited by S. A. Rice and A. R. Dinner (Wiley, Hoboken, NJ, 2012), Vol. 150, pp. 187–253.
- [7] T. Sakaue, *Polymers* **8**, 424 (2016).
- [8] K. Norregaard, R. Metzler, C. M. Ritter, K. Berg-Sørensen, and L. B. Oddershede, *Chem. Rev.* **117**, 4342 (2017).
- [9] V. Klippenstein, M. Tripathy, G. Jung, F. Schmid, and N. F. A. van der Vegt, *J. Phys. Chem. B* **125**, 4931 (2021).
- [10] S.-H. Chung and M. Roper, *Biophys. Rev. Lett.* **14**, 171 (2019).
- [11] F. Höfling and T. Franosch, *Rep. Prog. Phys.* **76**, 046602 (2013).
- [12] S. C. Kou and X. S. Xie, *Phys. Rev. Lett.* **93**, 180603 (2004).
- [13] S. C. Kou, *Ann. Appl. Stat.* **2**, 501 (2008).
- [14] M. Lysy, N. S. Pillai, D. B. Hill, M. G. Forest, J. W. R. Mellnik, P. A. Vasquez, and S. A. McKinley, *J. Am. Stat. Assoc.* **111**, 1413 (2016).
- [15] I. Goychuk, *Phys. Rev. E* **80**, 046125 (2009).
- [16] J.-H. Jeon and R. Metzler, *Phys. Rev. E* **81**, 021103 (2010).
- [17] E. B. Postnikov and I. M. Sokolov, *J. Phys. A: Math. Theor.* **57**, 055002 (2024).
- [18] M. Sahimi, *Phys. Rep.* **306**, 213 (1998).
- [19] X. Peng, Y. Zhang, H. Chu, Y. Li, D. Zhang, L. Cao, and G. Li, *J. Chem. Theory Comput.* **12**, 2973 (2016).
- [20] L. Dagdug, A. M. Berezhkovskii, V. Y. Zitserman, and S. M. Bezrukov, *Phys. Rev. E* **103**, 062106 (2021).
- [21] L. Dagdug, A. M. Berezhkovskii, and S. M. Bezrukov, *J. Phys. Chem. B* **127**, 7291 (2023).
- [22] X. Shao, M. H. Sørensen, X. Xia, C. Fang, T. H. Hui, R. C. C. Chang, Z. Chu, and Y. Lin, *J. R. Soc., Interface* **17**, 20200331 (2020).
- [23] M. Nilsson, J. Lätt, F. Ståhlberg, D. van Westen, and H. Hagslätt, *NMR Biomed.* **25**, 795 (2012).
- [24] H.-H. Lee, S. N. Jespersen, E. Fieremans, and D. S. Novikov, *Neuroimage* **223**, 117228 (2020).
- [25] C. Marchadour, E. Brouillet, P. Hantraye, V. Lebon, and J. Valette, *J. Cerebral Blood Flow Metab.* **32**, 2153 (2012).
- [26] C. Ingo, W. Brink, E. Ercan, A. G. Webb, and I. Ronen, *Brain Struct. Funct.* **223**, 3841 (2018).
- [27] A. Döring and R. Kreis, *Neuroimage* **202**, 116075 (2019).
- [28] C. Ligneul, C. Najac, A. Döring, C. Beaulieu, F. Branzoli, W. T. Clarke, C. Cudalbu, G. Genovese, S. Jbabdi, I. Jelescu, D. Karampinos, R. Kreis, H. Lundell, M. Marjańska, H. E. Möller, J. Mosso, E. Mougél, S. Posse, S. Ruschke, K. Simsek *et al.*, *Magn. Reson. Med.* **91**, 860 (2024).
- [29] C. Nicholson and S. Hrabětová, *Biophys. J.* **113**, 2133 (2017).
- [30] C. Nicholson, *J. R. Soc., Interface* **20**, 20230223 (2023).
- [31] Z.-G. Wang, L. Wang, D. C. Lamb, H.-J. Chen, Y. Hu, H.-P. Wang, D.-W. Pang, and S.-L. Liu, *Nano Lett.* **21**, 642 (2021).
- [32] E. B. Postnikov, A. I. Lavrova, and D. E. Postnov, *Int. J. Mol. Sci.* **23**, 12401 (2022).
- [33] P. Kalinay and J. K. Percus, *J. Chem. Phys.* **122**, 204701 (2005).
- [34] P. S. Burada, G. Schmid, P. Talkner, P. Hänggi, D. Reguera, and J. M. Rubí, *BioSystems* **93**, 16 (2008).
- [35] A. M. Berezhkovskii, L. Dagdug, and S. M. Bezrukov, *J. Chem. Phys.* **143**, 164102 (2015).
- [36] E. Locatelli, V. Bianco, C. Valeriani, and P. Maggaretti, *Phys. Rev. Lett.* **131**, 048101 (2023).
- [37] R. M. Bradley, *Phys. Rev. E* **80**, 061142 (2009).
- [38] E. Yariv, H. Brenner, and S. Kim, *SIAM J. Appl. Math.* **64**, 1099 (2004).
- [39] *Handbook of Mathematical Functions with Formulas, Graphs, and Mathematical Tables*, edited by M. Abramowitz and I. A. Stegun (National Bureau of Standards, Washington, DC, 1964).
- [40] R. Kupferman, *J. Stat. Phys.* **114**, 291 (2004).
- [41] P. Hänggi, in *Stochastic Dynamics*, edited by L. Schimansky-Geier and T. Pöschel (Springer, Berlin, 2007), pp. 15–22.
- [42] R. Zwanzig, *J. Phys. Chem.* **96**, 3926 (1992).